Cerebral Cortex Advance Access published August 9, 2012

Cerebral Cortex
doi:10.1093/cercor/bhs248

Effects of Aging on Properties of the Local Circuit in Rat Primary Somatosensory Cortex (S1) In Vitro

Peter Hickmott[1] and Hubert Dinse[2]

[1]Department of Psychology and Interdepartmental Neuroscience Program, University of California Riverside, Riverside, CA 92521, USA and [2]Department for Neuroinformatics, Neural Plasticity Lab, Ruhr University Bochum, Germany

Address correspondence to Peter Hickmott, Department of Psychology, UCR, Riverside, CA 92521, USA. Email: peter.hickmott@ucr.edu

During aging receptive field properties degrade, the ability of the circuit to process temporal information is impaired and behaviors mediated by the circuit can become impaired. These changes are mediated by changes in the properties of neural circuits, particularly the balance of excitation and inhibition, the intrinsic properties of neurons, and the anatomy of connections in the circuit. In this study, properties of thalamorecipient pyramidal neurons in layer 3 were examined in the hindpaw region of rat primary somatosensory cortex (S1) in vitro. Excitatory and inhibitory postsynaptic currents (IPSCs) resulting from trains of electrical stimulation of thalamocortical afferents were recorded. Excitatory postsynaptic currents were larger in old S1, but showed no difference in temporal dynamics; IPSCs showed significantly less suppression across the train in old S1, partly due to a decrease in $GABA_B$ signaling. Neurons in old S1 were more likely to exhibit burst firing, due to an increase in T-current. Significant differences in dendritic morphology were also observed in old S1, accompanied by a decrease in dendritic spine density. These data directly demonstrate changes in the properties of the thalamorecipient circuit in old S1 and help to explain the changes observed in responses during aging.

Keywords: EPSC, IPSC, $GABA_B$, paired-pulse depression, T-current

Introduction

During aging many sensory, motor, and cognitive behaviors decline. Corresponding neural circuits at all levels of the nervous system are subject to significant change in their physiological, anatomical, and molecular properties. Although we are beginning to understand some of the cellular and molecular changes that occur during aging, the changes in circuit organization and properties are mostly unknown.

One prominent change in the organization of cortical circuits during aging is degradation of normal receptive field (RF) properties. Expansion and disruption of RFs in old animals have been observed in primary somatosensory (S1), auditory (A1), and visual cortices (V1). In each case, there is also a decline in normal perceptual function of the corresponding sensory modality (Spengler et al. 1995; Schmolesky et al. 2000; Mendelson and Ricketts 2001; Godde et al. 2002; Mendelson and Wells 2002; David-Jurgens et al. 2008). In humans it is more difficult to measure RF properties, but expansion of the hand representation has been demonstrated in association with both a decrease in tactile acuity (Kalisch et al. 2009) and an increase in 2-point discrimination (Weiss et al. 2004). Another important aspect of brain circuits is their ability to process temporally complex stimuli, such as repetitive stimulus trains. The ability of cortical areas to effectively follow trains of stimuli can also be impaired during normal aging (Mendelson and Ricketts 2001; Mendelson and Wells 2002; Dinse 2006).

RF structure and the temporal dynamics of responses are shaped by the balance of excitation and inhibition. Excitation serves to activate neurons via ascending inputs and, at least in cortex, feed-forward excitation tends to amplify and spread excitation; inhibition, particularly feed-forward, constrains the spread of excitation and shapes the overall RF structure. These synaptic properties then interact with intrinsic properties of the neuron to determine its output (Shepherd 2004). Thus, experimentally blocking inhibition or enhancing excitation typically causes expansion of RFs (Hicks et al. 1986; Chowdhury and Rasmusson 2002). Temporal dynamics rely on the temporal properties of both excitation and inhibition. Both excitatory and inhibitory synapses exhibit modulation during repetitive activation. This modulation manifests as either facilitation (i.e. responses become larger during the train) or suppression (i.e. responses become smaller). The relative rates and amounts of these 2 processes, along with the intrinsic excitability of the cell, will determine whether the overall spiking response (output) of a given cell will by enhanced or depressed during a train (Galarreta and Hestrin 1998).

An important hypothesis concerning the effects of aging on brain circuits is that there is a general loss or disruption of normal inhibitory control (Dinse 2006; Wong et al. 2006; Caspary et al. 2008). Initial support for this idea was obtained based on decreases in the expression of various molecular markers for inhibition, such as GAD65 and γ-aminobutyric acid (GABA) (Mora et al. 2007), and on reductions in the density of putative inhibitory synapses. More direct evidence was obtained in hippocampus and cortex using in vitro electrophysiology (Barnes 1994; Wong et al. 2000; Luebke et al. 2004), and infusions of GABA agonists and antagonists (Leventhal et al. 2003). In humans, electroencephalography measurements and stimulation studies have provided evidence for decreased inhibition in old cortex (Dustman et al. 1996; Weiss et al. 2004). However, measures of synaptic excitation also change during aging. For example, densities of glutamate receptors are typically reduced in aged brain (Segovia et al. 2001), and the density of dendritic spines in aged hippocampus and cortex are significantly reduced (Segovia et al. 2001; Rosenzweig and Barnes 2003). As spines are major targets of excitatory synapses, this likely reflects an overall reduction in excitation. Such a decrease in excitation can be directly observed in area CA1 of hippocampus (Barnes 1994). The intrinsic excitability of neurons can also change during aging, with both increases and decreases in excitability documented in different cell types (Chang et al. 2005; Luebke and Chang 2007).

© The Author 2012. Published by Oxford University Press. All rights reserved.
For Permissions, please e-mail: journals.permissions@oup.com

Studies in the hindpaw representation of rat S1 have begun to address the changes in responsiveness that occur during normal aging. Initially, it was found that the size of the hindpaw RFs is significantly expanded in old rats (Spengler et al. 1995; Godde et al. 2002; David-Jurgens et al. 2008). It was hypothesized that the expansion was due to a general loss of inhibition, as similar expansions also occur when inhibition is experimentally blocked (Hicks et al. 1986; Chowdhury and Rasmusson 2002). In support of this hypothesis, the number of parvalbumin-positive interneurons in hindpaw S1 decreased in old S1 (Jürgens and Dinse 1998). A subsequent study was performed to examine the responses in S1 to pairs of tactile stimuli to the hindpaw (David-Jurgens and Dinse 2010). The amount of this paired-pulse depression was reduced in old S1, suggesting possible enhancement of inhibition. These studies were recently extended to trains of tactile stimuli to the hindpaw (David-Jurgens and Dinse 2008). Again, suppression of responses was observed across the train in adult and old animals. The amount of suppression in the aged animals was larger for a subset of those examined, consistent with a change in suppression of inhibition.

As these recordings were of spikes in intact animals, it is impossible to determine whether the change in response suppression in aged S1 was due to a change in synaptic excitation or inhibition and/or changes in intrinsic excitability. In order to examine these factors directly, an in vitro slice preparation from hindpaw S1 was used. In these slices, the ascending thalamocortical fibers were electrically stimulated to evoke excitatory and inhibitory postsynaptic currents (EPSCs and IPSCs) in thalamorecipient pyramidal cells of deep layer 3. Trains of stimuli were used to compare the short-term dynamics of EPSCs and IPSCs in adult (4–7 months old) and old (27–32 months old) rats. EPSCs were found to have larger amplitudes in old rats, but did not differ in their train dynamics; IPSCs, however, showed less suppression of their responses across stimulus trains in the old rats, and this decreased suppression was mediated in part by a reduction in $GABA_B$ signaling. General increases in the intrinsic excitability of these neurons were also observed with age, associated with an increase in *t*-current mediated burst firing. Finally, differences in dendritic anatomy and spine density were also observed in old S1.

Materials and Methods

Experiments were performed on young adult (4–7 months) and aged (27–32 months) FBNF1 hybrid rats. All animal procedures are consistent with NIH guidelines and were approved by the Institutional Animal Care and Use Committee at the University of California Riverside. All chemicals were purchased from Sigma-Aldrich Chemical Co. unless otherwise indicated.

In Vivo Recording

Rats were anesthetized with pentobarbital (50 mg/kg, intraperitoneal) and mounted in a stereotaxic frame. Supplemental doses of anesthetic were administered as needed. Lidocaine was injected subcutaneously around wound margins and at pressure points. Rectal temperature was maintained at 38°C with a heating pad.

S1 was exposed via a wide craniotomy centered on Bregma, the dura was removed, and the cortex covered with silicone oil. A computer image of the brain surface was recorded using a CCD camera and appropriate software (Pixera). Carbon-fiber electrodes (10 μm fiber diameter) were used for response mapping. The hindpaw and forepaw were stimulated with a fine glass probe to elicit cutaneous responses in S1. The location of penetrations was recorded on the computer image of the cortex by using landmarks of the surface vasculature. The medial-lateral extent of the rostral hindpaw representation was determined so that the middle of the hindpaw representation could be located. Two points in the middle of the hindpaw representation were then marked with DiI: one typically 300–500 μm caudal to the rostral border of the representation, and the second 500 μm caudal to the first point. For marking, the recording electrode was repeatedly dipped in a 1–2% DiI solution (in ethanol) and DiI crystals allowed to deposit on the electrode (DiCarlo et al. 1996). This electrode was used to mark the sites in the middle of the rostral hindpaw representation.

In Vitro Recording

After marking, the animal was decapitated, the brain rapidly removed, and 400-μm–thick coronal slices cut on a vibrating microtome (VT1000, Leica) from the marked region of cortex. Marked sites were visualized using an epifluorescence microscope and their location was determined in relation to visible landmarks in the slice. These slices were maintained in standard mammalian artificial cerebrospinal fluid (ACSF; in mM: NaCl, 119; KCl, 2.5; NaH_2PO4, 1.25; $MgSO_4$, 1.3; $CaCl_2$, 2.5; $NaHCO_3$, 26.2; glucose, 11; saturated with 95%O_2/5%CO_2) for intracellular recording at 30.5°C. Note that brains were sectioned in ACSF in which the NaCl was replaced by isoosmotic sucrose to which 100 μM Dl-4-amino-5-phosphonovaleric acid (APV) was added. The slices were incubated in this sucrose-replacement ACSF for at least 45 minutes after sectioning and were then transferred to standard ACSF for at least 45 min before recording.

Neurons for recording were obtained using blind whole-cell recording (Blanton et al. 1989) from a region near the mark (<200-μm distant; means: 130 ± 16 μm for old and 115 ± 14 for adult) and between 500 and 600 μm (means: 558 ± 10 μm for old and 569 ± 10 μm for adult) from the cortical surface. Patch electrodes were pulled on a Flaming/Brown puller (Sutter Instruments) to an internal tip diameter of 1.5–2.5 μm. Electrodes were filled with either a Cs-based solution (for recording synaptic currents) or a K-based (for recording intrinsic properties). The solution consisted of (in mM): Cs-Gluconate or K-gluconate, 128; CsCl or KCl, 7; EGTA, 1; HEPES, 10; Mg-ATP, 2; Na-GTP, 0.2; biocytin, 0.2%; pH 7.0–7.4. Filling solution for recording PSCs also contained 10 mM QX-314 to block action potentials (APs). Electrodes had tip resistances of 3–6 MΩ. Only neurons with initial resting potentials more negative than −55 mV and stable input resistances of >50 MΩ were used. Any recordings in which the access resistance changed by >15% during the course of the experiment were not used for analysis. Recordings were amplified using an Axoclamp 2B amplifier (Axon Instruments) in voltage-clamp or current-clamp mode, digitized at 15 kHz for synaptic currents and 40 kHz for intrinsic properties (National Instruments), and saved to the hard disk of a personal computer (Macintosh G4) using the IgorPro (Wavemetrics, Inc) data acquisition system.

Analysis of PSCs

EPSCs were isolated by recording at the chloride reversal potential (~−55 mV), whereas IPSCs were isolated by recording at the reversal potential for glutamate (~0 mV). Note that in order to stably hold V_M at 0 mV, all PSC recordings were performed in the presence of 15 μM nifedipine in order to block large L-type calcium currents. In some cases, IPSCs were further isolated by bath-application of 15 μM CNQX and 100 μM APV.

Stimulation was applied via bipolar parylene-coated tungsten electrodes (resistance ~1 MΩ) with a tip separation of ~50 μm (FHC, Inc, Bowdoin, ME). For most experiments the stimulating electrode was placed directly below the recorded neuron between 1600 and 2200 μM from the cortical surface (mean: 1678 ± 51 μm for old, 1679 ± 48 μm for adult) in layer 6 to stimulate primarily thalamocortical inputs. In experiments in which horizontal connections were stimulated, the electrode was placed at the same distance from the cortical surface as the recorded cell at approximately 200 μm medial or lateral. Stimuli consisted of single pulses (100 μs duration) or short trains (15 pulses of duration 100 μs) at interpulse intervals (IPIs) of 35, 50, 100,

200, and 400 ms. For determining the minimal PSC amplitude, single PSCs were evoked at a stimulus intensity that resulted in a failure rate of >20%. Stimulus intensity was then increased incrementally until the maximal PSC amplitude was reached. Input/output (I/O) plots were generated from these data (Fig. 1). Properties of spontaneous PSCs (sPSC) were determined from unstimulated records. sPSC mean amplitude and frequency were determined from 30–50 individual spontaneous events. For trains, stimulus intensity was adjusted to evoke PSCs of approximately half the maximal PSC amplitude for that particular cell. For each train of PSCs, the paired-pulse ratio (PPR) was defined as the ratio of the amplitude of the second PSC to the first; the steady-state ratio (SSR) was defined as the ratio of the mean amplitude of the last 3 PSCs to the first. In some cases, CGP 55845 (5 μM; Tocris Bioscience) was bath applied to slices for at least 15 min so that the effects of blocking $GABA_B$ receptors could be observed.

Analysis of Intrinsic Properties

Neurons were current-clamped at −70 mV, and 500 ms duration square pulses of current (both negative and positive) were injected at 0.2 Hz. I/O relations were determined for sub- and supra-threshold currents, typically starting at −1.5 nA and increasing in fixed steps to a maximum of −3 nA. The amplitude of single APs was measured from the inflection point between the initial passive depolarization and the beginning of the spike to the peak of the spike; the AP threshold was measured from baseline to inflection point and the AP half width was measured as the duration of the AP at 50% of its amplitude (Fig. 5*A*). Trains of APs were quantified by plotting the number of APs for each suprathreshold current. From these I/O plots, the maximum number of APs was determined. These I/O plots were well fit by an exponential function, so when plotted semi-logarithmically they were well fit by a straight line. The slope of that line was used as a measure of the rate of rise of the I/O plot (Fig. 4*G*).

In all cases, there were fast afterhyperpolarizations (fAHP) following APs, and in some cases there were also fast afterdepolarizations (ADP; see Fig. 6*A*). fAHP amplitude was measured from the inflection point to the rapid, hyperpolarizing peak of the AHP (Fig. 6*A*, bottom right). The ADP amplitude was measured from the fAHP to the peak of the ADP (Fig. 6*A*). The medium AHP (mAHP) and slow AHP (sAHP) were evoked by a train of 20–30 APs in cells that were depolarized to −55 mV. The mAHP amplitude was measured from baseline to the peak of the hyperpolarization after the AP train, whereas the sAHP amplitude was measured at 450 ms after the offset of the AP train (Fig. 6*D*). A measure of the duration of the mAHP was obtained by fitting an exponential function from the peak of the mAHP to the end of the trace (at 450 ms after the offset of the AP train) and determining the fall-time tau of the function. The duration of the sAHP was estimated by fitting a line to the falling phase of the sAHP between 100 and 450 ms after the offset of the AP train and extrapolating that line until it intersected with baseline; the amount of time to this intersection was taken as the duration of the sAHP.

For subthreshold potentials, the peak amplitude and the amplitude at 400 ms of the current pulse (steady-state) were determined for each current amplitude and plotted. This I/O plot was well fit by a straight line for both peak and steady-state measures, and the slope of the line was used as an overall measure of subthreshold potential amplitude. In some cells, there was a pronounced depolarizing "hump" on the positive potential just below threshold (Fig. 4*B*). These potentials were quantified as the difference between the peak of the "hump" and the steady-state amplitude (measured at 400 ms).

Analysis of Neuronal Morphology

After recordings, slices were fixed in 10% formalin overnight at 4°C, the slices were rinsed in phosphate buffer, permeablized with 0.5% Triton-X (30 min at room temperature), and incubated with ALEXA-488 streptavidin (Molecular Probes) overnight at 4°C. Sections were mounted in 90% glycerol with 4% *N*-propyl gallate added. Filled neurons were imaged using laser-scanning confocal microscopy (Zeiss 510). Images of dendrites were acquired at 10× with a 2× zoom. In all cases, the gain and black level were adjusted so that most of the labeled dendrites were saturated. Z-stacks were obtained for the entire depth of the cell and 2-dimensional projections of neuronal morphology were derived using the maximal pixel intensity at each point in the X–Y plane. Dendritic morphology was analyzed using the Scholl analysis (Hickmott and Merzenich 1999; Hickmott and Steen 2005). In this analysis, concentric circles were overlaid on the image of a neuron at 20 μm intervals centered on the soma; the number of intersections of each circle with labeled processes was determined for the entire neuron and also independently for the apical and basal dendrites. Apical dendrites were defined as all dendrites that branched from the primary apical dendrite, whereas basal dendrites were defined as those the branched ultimately from the soma. The number of branch points, total length of dendrites, and length of the

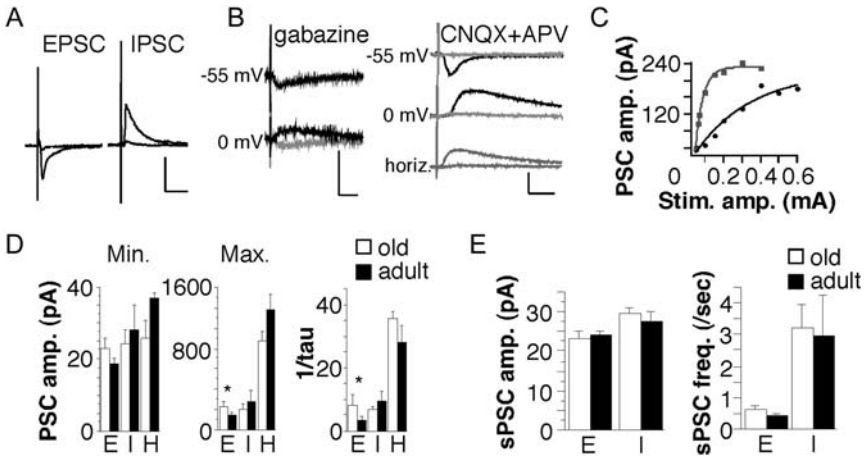

Figure 1. Amplitudes of thalamocortical and spontaneous PSCs in adult and old S1. (*A*) Examples of minimal and maximal amplitude thalamocortical EPSCs (left) and thalamocortical IPSCs (right) from the same cell of an adult. Scale bar: 200 pA, 50 ms. (*B*) Pharmacological characterization of PSCs. Bath application of 5 μM gabazine (left traces) was used to block IPSCs and 10 μM CNQX plus 100 μM DL-APV (right traces) was used to block EPSCs. Black traces are before block and gray traces are in the presence of the indicated blocker(s). All traces are the average of 3 individual records; all traces were evoked by thalamocortical stimulation, except for the bottom right traces ('horiz'), which were evoked by horizontal stimulation close to the cell (~200 μm distant). Scale bars: 20 pA, 20 ms. (*C*) Input/output curves for EPSCs (black circles) and IPSCs (gray squares) from a single neuron. The lines are the best exponential fit to each. (*D*) Mean amplitudes of minimal-amplitude PSCs (left), mean amplitudes of maximal-amplitude PSCs (middle), and mean 1/tau of the exponential fit to the I/O curve (right) for thalamocortical EPSCs (*E*), thalamocortical IPSCs (*I*) and horizontal IPSCs (*H*) in old (white bars) and adult (black bars) rats. $N = 11$ cells for old and 10 cells for adult for thalamocortical and $n = 8$ cells for old and 8 cells for adult for horizontal PSCs. Asterisks represent significant difference between old and adult means (Student's *t*-test, $P < 0.05$). (*E*) Mean amplitudes (left) and frequencies (right) of spontaneous EPSCs (*E*) and IPSCs (*I*) from old (white bars) and adult (black bars) rats. $N = 14$ cells for old and 14 cells for old animals.

longest dendrite were also determined. Dendritic spines were imaged at 40× or 63× in 3 locations: basal dendrites, primary dendrites, and apical tuft dendrites. Care was taken to acquire data from dendrites that were an equivalent distance from the soma (for basal and primary dendrites) or from the primary dendrite (for apical tuft dendrites). In each case, the 2-dimensional projection of the complete Z-series through that dendrite was used to determine the spine density. The total number of spines along a 50 μm length of dendrite was counted manually for each of the 3 locations.

Statistics

All data are reported as mean ± standard error mean. Statistical significance was determined either by planned Students' *t*-tests (for 2 means) or factorial analysis of variance (ANOVA) followed by individual comparisons using Fisher's protected least-squares difference (for >2 means); $P < 0.05$ was taken as significant.

Results

A total of 41 cells (21 for PSC analysis and 20 for AP analysis) were analyzed in 16 young adult rats (4–7 months old, mean 5.0) and 42 cells (21 for PSC analysis and 21 for AP analysis) in 15 old rats (26–32 months old, mean 29.1). All recordings reported in this paper were from pyramidal cells in deep layer 3 or 4 (Fig. 8). Resting potential and input resistance were compared separately for PSC recordings (using Cs-gluconate filling solution) and AP recordings (using K-gluconate filling solution). In both cases, the mean resting potential and input resistance were not significantly different between adult and old rats (resting potential: −67.7 ± 1.4 [Cs-gluconate] and −69.8 ± 1.4 [K-gluconate] mV for old and −69.4 ± 1.6 [Cs-gluconate] and −67.1 ± 1.3 [K = gluconate] mV for adult; input resistance: 112.6 ± 5.8 [Cs-gluconate] and 115.9 ± 11 [K-gluconate] MΩ for old and 124.9 ± 8.5 [Cs-gluconate], and 107.9 ± 10.2 [K-gluconate] MΩ for adult). In initial experiments, it proved impossible to stably voltage-clamp neurons in old rats to 0 mV, as large, sporadic inward currents were consistently activated (data not shown). As they were large and noninactivating, it was assumed that they were L-type calcium currents; this was confirmed as they were blocked by bath-applied 15 μM nifedipine. Thus, all experiments involving analysis of PSCs were performed in the presence of 15 μM nifedipine.

Properties of PSC Trains

PSCs evoked in adult and old S1 generally resembled each other closely. An example of typical minimal and maximal PSCs for an adult animal is shown in Figure 1*A*. The identities of the PSCs as EPSCs and IPSCs was confirmed pharmacologically ($n = 5$ neurons). Bath application of the $GABA_A$ antagonist, gabazine (5 μM, left traces in Fig. 1*B*), blocked the PSC evoked at ∼0 mV (left, bottom traces), but did not affect the PSC evoked at approximately −55 mV (left, top traces). Note that only small stimulus intensities could be used in the presence of gabazine, as larger stimuli resulted in uncontrolled paroxysmal activity in the disinhibited slice. Glutamate receptors were blocked by a combination of 10 μM CNQX and 100 μM DL-APV (Fig. 1*B*, right traces). This drug combination blocked the PSC evoked at approximately −55 mV (right, top traces) and the PSC evoked at approximately 0 mV (right, middle traces). We hypothesized that the block of the putative EPSC (top traces) was due to the block of direct, thalamocortical inputs onto the pyramidal cell recorded from and that the block of the putative IPSC (middle traces) was due to the block of thalamocortical inputs onto inhibitory interneurons that then synapsed onto the pyramidal cell. When we directly activated inhibitory connections onto the recorded cell by stimulating close to the recorded cell (Fig. 1*B*, right traces, bottom), CNQX plus APV did not block the PSC recorded at approximately 0 mV (upward current), but did block the PSC recorded at approximately −55 mV (flat trace). Thus, the PSC evoked at approximately −55 mV was confirmed as an EPSC and the PSC evoked at approximately 0 mV was confirmed as an IPSC.

To assess the relative amplitudes of PSCs, I/O plots were generated by evoking PSCs from minimal to maximal amplitude (Fig. 1*C*). The best exponential fit was calculated for these I/O plots (lines in Fig. 1*C*); 1/tau of this fit line was used as a measure of the rate of rise of the exponential function. For EPSCs, the amplitude of minimal PSCs did not differ between adult and old; however, maximal amplitudes and 1/tau were larger in old versus adult rats. For IPSCs (both those evoked by thalamocortical and horizontal stimulation), these measures were not different between old and adult (Fig. 1*D*). sPSC were also evaluated. The amplitudes of sEPSCs and sIPSCs did not differ significantly from each other between adult and old animals (Fig. 1*E*, left). Note that the amplitudes of sPSCs also did not differ significantly from the corresponding minimal PSC (Fig. 1*D*, left). The frequencies of sPSCs also did not differ significantly between old and adult animals (Fig. 1*E*, right).

Trains of stimuli evoked trains of PSCs that mostly showed depression throughout the train (Fig. 2*A*). For short IPIs (35, 50 ms), paired-pulse facilitation was observed in some cases, particularly for IPSCs (e.g. Fig. 2*A*1, *A*2). The magnitude of the depression was generally larger for IPSCs, particularly for the steady-state of the train (SSR; Fig. 2*A*). For EPSCs, there was no significant difference in the amount of depression for either rapid (PPR) or steady-state (SSR) depression between old (Fig. 2*B*1, white bars) and adult (Fig. 2*B*1, black bars) animals at any of the IPIs examined. For IPSCs evoked by both thalamocortical stimulation (Fig. 2*B*2) and horizontal stimulation (Fig. 2*B*3), depression was greater in adult animals (black bars) than old ones (white bars) for most IPIs, particularly for the steady-state depression (SSR).

One important mechanism underlying suppression of IPSCs during repetitive stimulation in the cortex is the activation of $GABA_B$ autoreceptors on presynaptic inhibitory terminals (Zucker and Regehr 2002). We tested the hypothesis that the decreased suppression of IPSCs observed in old animals (Fig. 2) was caused by a reduction in this $GABA_B$ signaling. When an antagonist of $GABA_B$ receptors (5 μM CGP 55845) was bath applied to slices, there was typically a decrease in suppression of IPSCs during a train, but no apparent effect on EPSC suppression (Fig. 3*A*, gray traces). This effect was quantified for each IPI by taking the post-CGP/pre-CGP ratio of PPR and SSR for each IPI. Thus, a ratio of 1 would indicate no effect of CGP on suppression. As shown in Fig. 3*B* for the entire population, EPSCs showed no significant effects of CGP on either PPR or SSR for any IPI (Fig. 3*B*, left). However, significant effects of CGP (ratios >1) were observed for IPSCs only in adult animals and for short IPIs (35, 50, 100 ms; Fig. 3*B*, right); old animals showed little-to-no effect on IPSC suppression (ratios ∼1). The ratios were significantly larger in adult rats than for old rats at 35, 50, and 100 ms IPIs for PPR

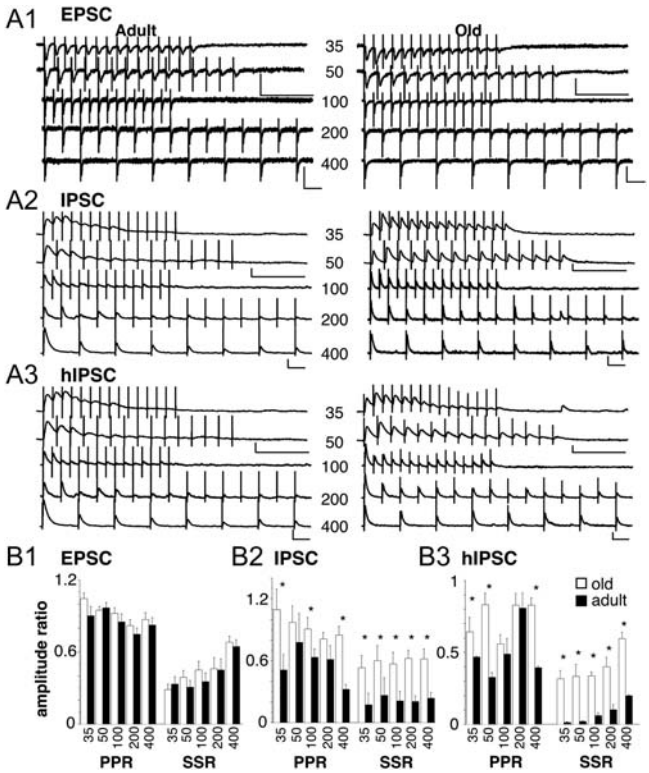

Figure 2. PSCs evoked by trains of stimuli at various IPIs. For A1-A3 traces on the left are from adult animals and on the right from old animals. IPIs are in msec as indicated. The scale bars represent 100 pA and 100 ms. Note the change in scale between the top 2 traces (35 and 50 ms IPI) and the bottom three (100, 200, and 400 ms IPI, A1) Examples of EPSCs evoked by stimulation of thalamocortical afferents, A2) Examples of IPSCs evoked by stimulation of thalamocortical afferents. These IPSCs were recorded in the same cell as the EPSCs in A1, A3, examples of IPSCs evoked by stimulation of horizontal afferents. B1–B3: Effects of repetitive stimulation on mean PPR and SSR for PSCs from adult (black bars) and old (white bars) animals for the indicated IPIs. Asterisks represent mean values that differ significantly between corresponding old and adult values (Student's *t*-test, $P < 0.05$). B1: Mean PPR and SSR values for thalamocortical EPSCs. $N = 12$ cells for old and 13 cells for adult. B2: Mean PPR and SSR values for thalamocortical IPSCs. $N = 11$ cells for old and 11 cells for adult. B3: Mean PPR and SSR values for horizontal IPSCs. $N = 9$ cells for old and 9 cells for adult.

and SSR. Thus, the effectiveness of $GABA_B$ autoreceptors was less in old rats than in adults, which would explain the reduced IPSC suppression observed (Fig. 2), at least for short IPIs.

Properties of Action Potentials

Basic firing properties of layer 3 pyramidal cells were also examined in old and adult cortex by injecting 500-ms–long square pulses of current of various intensities (subthreshold to maximal) from a base membrane potential of −70 mV. APs were evoked by positive currents and the characteristics of single APs (Fig. 5) and trains (Fig. 4) were examined. These neurons exhibited 2 different firing patterns: regular spiking (RS) in which the interspike intervals (ISIs) generally increase gradually during the train (Fig. 4*A*, right); and initial bursting (IB) in which cells fired a short burst (>3) of APs at high frequency followed by a gradual increase in ISI (Fig. 4*A*, left). These types were categorized objectively by examining the third ISI (Fig. 4*E*, right); cells in which this parameter was <5 ms were categorized as IB. IB cells had significantly smaller third ISIs than RS cells, although there was no difference between old and adult animals (Fig. 4*E*, right, −70; $F = 12.63$, $P < 0.0001$). The percentage of IB cells was larger in old animals (52% in old vs. 30% in adult). Burst firing in cortical neurons is mediated by the interplay of various intrinsic currents, particularly Ca^{2+} currents, persistent Na^+ currents, and K^+ currents (Amitai and Connors 1995). One important subtype of Ca^{2+} current for generating bursting in cortex is the low-threshold inactivating T-current (McCormick et al. 1985; Chen et al. 1996). The potential associated with T current could be observed on just-subthreshold responses as a transient depolarizing "hump" at the beginning of the response (Fig. 4*B*, left). The identity of this "hump" as the T-potential was confirmed in a few IB cells ($n = 5$) by blocking the potential with 100 μM Ni^{2+} (Fig. 4*D*). This T-potential was observed strongly in IB neurons, but not in RS neurons (Fig. 4*B*). In fact, for both old and adult animals, the mean amplitude of the T-potential was significantly larger in IB cells than in RS (Fig. 4*C*). Overall, the T-potential amplitude was significantly larger in old animals (4.6 ± 0.6 mV) than in adult (2.9 ± 0.7 mV); however, when the data were separated based on the firing pattern (IB vs. RS), the difference ($F = 25.48$, $P < 0.0001$) was only observed for RS cells (Fig. 4*B*, hatched vs. black bars). IB cells showed no significant difference (Fig. 4*B*, white vs. gray bars).

The role of this T-potential in generating burst firing was confirmed by depolarizing IB cells to −55 mV, which will inactivate T current and has been shown to convert burst-firing cells to regular-spiking cells in cortical neurons (McCormick et al. 1985; Chen et al. 1996). Figure 4*E* (left) shows an example of the early part of the AP train from an IB cell at −70 mV (bottom black trace); when the cell was depolarized to −55 mV, the initial burst was lost and it was classified as an RS cell (Fig. 4*D*, top gray trace). Depolarization consistently changed the firing characteristics of IB cells, as measured by the duration of the third ISI (Fig. 4*E*, right, white and gray bars). Depolarization did not change firing category or the duration of the third ISI for RS cells (Fig. 4*E*, right, hatched and black bars). At −55 mV, unlike at −70 mV there was no significant difference among the third ISIs ($F = 2.00$, $P = 0.113$).

Spike trains were quantified by determining the maximum number of spikes evoked (Fig. 4*F*) and by plotting the number of spikes versus the amplitude of current injected Fig. 4*G*). These I/O plots could be well fit by a single exponential function (data not shown), so when plotted semilogarithmically they yielded a plot well fit by a straight line. The slope of this line was used as a measure of the rate of increase in spikes/nA of current (Fig. 4*G*). Neither of these measures was different between old and adult animals; when divided into IB and RS categories, IB cells tended to have larger maximal numbers of spikes and higher slopes, but the data were not significant (Fig. 4*F* [$F = 1.2$, $P = 0.32$]; Fig. 4*G* [$F = 1.48$, $P = 0.26$]). Thus, the differences between old and adult animals were mainly manifested in the early portion of the spike train, as a difference between bursting and nonbursting.

The characteristics of single APs evoked by a just suprathreshold current proved not to be significantly different between old and adult animals for either IB or RS cell types (Fig. 5). The threshold depolarization to evoke a spike (Fig. 5*B*, left [$F = 2.46$, $P = 0.078$]), the spike amplitude (Fig. 5*B*, middle [$F = 1.75$, $P = 0.17$]), and the width of the spike at one-half its amplitude (Fig. 5*B*, right [$F = 2.27$, $P =$

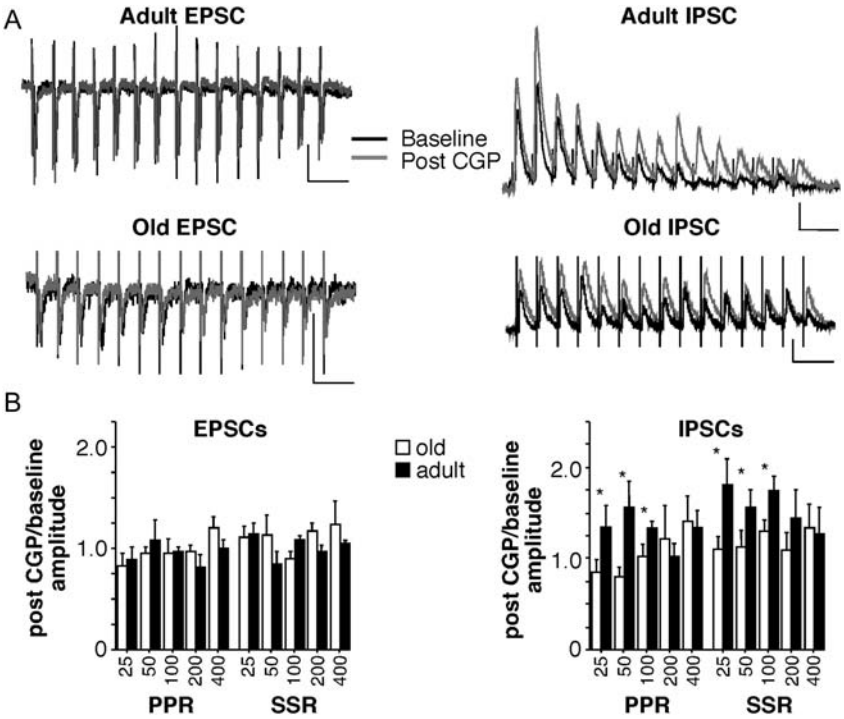

Figure 3. Effects of CGP 55845 on PSC trains. (*A*) Examples of trains of thalamocortical EPSCs (left) and IPSCs (right) from adult (top) and old (bottom) rats before (black traces) and during (gray traces) bath application of 5 μM CGP 55845. Scale bars represent 100 pA and 100 ms. (*B*) Quantification of effects of CGP 55845 on PPR and SSR for EPSCs (left) and IPSCs (right) at various IPIs for old (white bars) and adult (black bars) animals. PPR and SSR values were determined for each IPI and the ratio of the value during and before CGP 55845 was determined. $N = 9$ cells for old and $n = 10$ cells for adult. Asterisks represent mean values that differ significantly between corresponding old and adult values (Student's *t*-test, $P < 0.05$).

0.19]) were not significantly different for the 4 categories of neurons examined (one-way ANOVA).

An important determinant of single-spike and spike train properties is AHPs, mostly carried by various types of potassium currents. The AHPs are generally divided into fAHP, mAHP and sAHP (Sah 1996). fAHPs were quantified after single spikes (Fig. 6*A*, *B*), whereas mAHPs and sAHPs were quantified after trains of spikes (~20) and at −55 mV to enhance their amplitude (Fig. 6*D*, *E*). For many cells, there was also a transient ADP (arrowheads in Fig. 6*A*) after the single spike. The fAHP was measured from the inflection point of the spike to the peak of the rapid hyperpolarization after the spike (Fig. 6*A*, bottom right). Note that in some cases the mAHP obscured the fAHP so that only a slight notch indicated its amplitude (Fig. 5*A*, bottom left). Also, the ADP, when present, appeared to overlap with the fAHP; however, the amplitude of the ADP and fAHP was not correlated (data not shown), so we believe the measure of fAHP is appropriate. The ADP was measured from the initial hyperpolarization after the spike to the subsequent peak depolarization (Fig. 6*A*, top left). There was no significant difference in fAHP amplitude among the 4 groups (Fig. 6*B*, left [$F = 0.542$, $P = 0.66$]), whereas the ADP was smaller for RS cells than for IB cells for both adult and old animals (Fig. 6*C* [$F = 16.79$, $P < 0.0001$]). This pattern was very similar to that observed for the T-potential amplitude (Fig. 2*C*); however, the ADP was not a manifestation of the T-potential, as the ADP was not significantly reduced by depolarization to −55 mV (data not shown), unlike the T-potential (Fig. 4*E*). The mAHP was quantified from baseline to the peak hyperpolarization after a spike train at −55 mV (Fig. 6*D*). There was no significant difference in the mAHP for any of the conditions (Fig. 6*E* [$F = 0.19$, $P = 0.90$]). The sAHP amplitude was measured at 450 ms after the offset of the AP train (Fig. 6*D*), and there was no significant difference in the sAHP amplitude for any of the conditions (Fig. 6*E* [$F = 0.51$, $P = 0.68$]). The duration of the mAHP, as measured by the falling tau of the exponential fit, was significantly different between old and adult animals (487 ± 142 ms for old and 117 ± 19 ms for adult); the duration of the sAHP, as measured by linear extrapolation of the falling phase of the sAHP, was not different (1987 ± 241 ms for old and 1859 ± 1166 ms for adult). When divided into IB and RS categories, RS cells from old animals were significantly different from the other 3 categories (Fig. 6*F*, left plot [$F = 6.12$, $P = 0.002$]).

Possible differences in subthreshold responses were examined using both positive and negative current steps in old and adult animals for IB and RS cell types (Fig. 7*A*). The most obvious difference in these subthreshold potentials, the larger T-potential in IB cells and in old RS cells, has already been documented in Figure 4*B*, *C*. In order to assess the various parts of the subthreshold potentials over the entire range of currents, the amplitude of the potential was plotted against the injected current at the early peak of the current (peak) and at 400 ms after current initiation (steady-state, data not shown). These plots were well fit with a linear regression line for both peak and steady-state potentials, and the slope of this line was used as an overall measure of the subthreshold potentials. These slopes did not differ significantly among old and adult animals, nor IB and RS cells (Fig. 7*B* [peak $F = 1.55$, $P = 0.24$; steady-state $F = 1.39$, $P = 0.28$]). In order to remove any possible effect of the T-potential, the analysis was

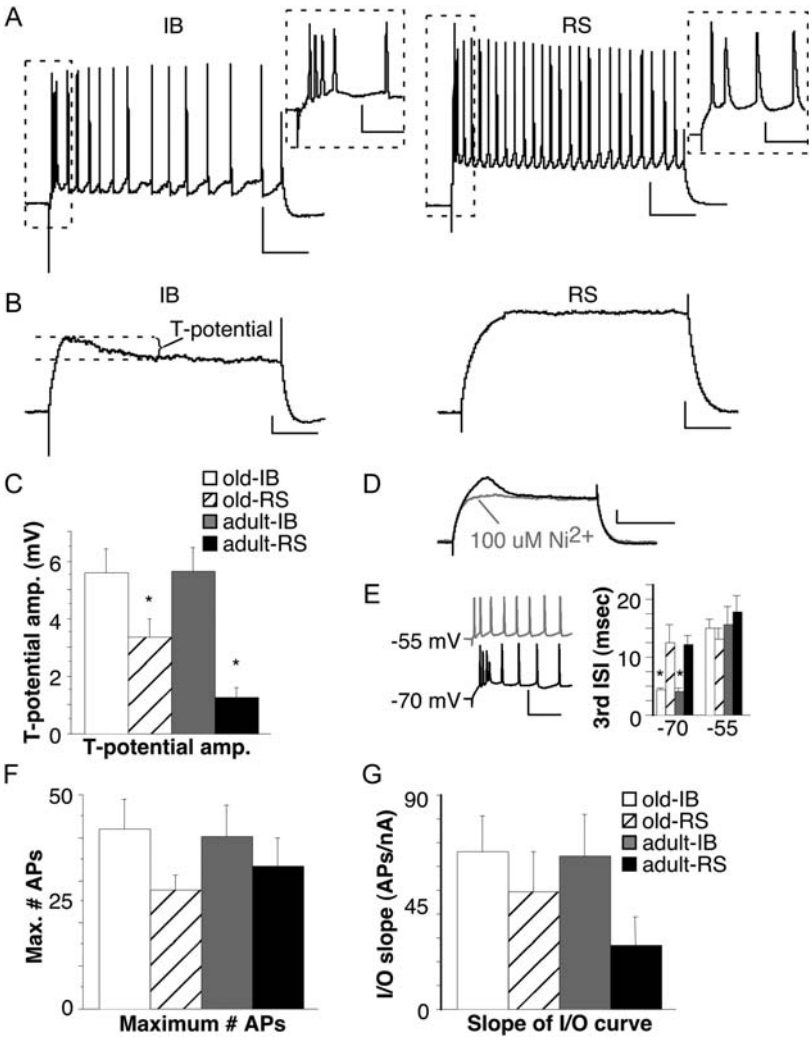

Figure 4. Differences in action potential trains in old and adult animals. $N = 21$ cells (11 IB and 10 RS) for old and 20 cells (6 IB and 14 RS) for adult. (*A*) Examples of initially-bursting (IB) and regular-spiking (RS) neurons from an old (left) and adult (right) rat. Scale bars represent 20 mV and 100 ms. The inset shows the boxed area at expanded time base (scale bars represent 20 mV and 10 ms). (*B*) Examples of the T-potential in an IB (left) and RS cell (right). Scale bars represent 5 mV and 100 ms. (*C*) Mean T-potential amplitude for old versus adult and IB versus RS cells. Asterisks represent means that differ significantly from the other 3 means (1-way ANOVA, followed by Fisher's protected least-squares difference (PLSD), $P < 0.05$). (*D*) Example of the effects of bath-applied Ni^{2+} (100 μM) on the T-potential. Scale bars represent 5 mV and 200 msec. (*E*) Depolarization from −70 mV (black trace) to −55 mV (gray trace) converted neurons from IB to RS firing patterns. Scale bars represent 40 mV and 50 ms. The plot (right) shows the mean length of the third ISI for old versus adult and IB versus RS cells. Means for IB cells are significantly smaller than for RS cells (asterisks) only for hyperpolarized cells (−70) not for depolarized (−55; 1-way ANOVA, followed by Fisher's PLSD, $P < 0.05$). (*F*) Mean maximum number of spikes for old versus adult and IB versus RS cells. (*G*) Mean slope of the spike I/O curve for old versus adult and IB versus RS cells.

repeated with the largest depolarizing subthreshold potential (which is when the T-potential was manifest) excluded from the plot. This exclusion had no significant effect on the outcome of the analysis presented in Figure 7*B*.

Properties of Dendrites and Spines

There were also differences in the morphology of the neurons in adult and old S1. All cells analyzed here had somata located in layer 4 or deep layer 3 (mean depth from the cortical surface: 558 ± 20 μm for old and 578 ± 18 μm for adult). All were typical pyramidal neurons with extensive basal and apical dendrites (Fig. 8*A*). A Scholl analysis (see Methods) was performed to measure the overall complexity of the dendritic arbors. Overall, the mean number of intersections was significantly greater in old animals than adult. This difference initially appeared to result just from an increased number of intersections in the apical dendrites of old animals (Fig. 8*B*). However, when the analysis was refined, examining the number of intersections for each 20-μm interval (Fig. 8*C*, *D*), a larger number of intersections was observed for adult animals for basal dendrites at approximately 100 μm from the soma (Fig. 8*C*), whereas a larger number was observed for older animals for apical dendrites between 60 and 180 μm (Fig. 8*D*). Scholl analysis is a measure of overall complexity and includes both length and branchiness; the total lengths of dendrites were longer for adult animals for all parts of the dendritic tree (Fig. 8*F*). The longest dendrite length was also larger for adult animals for the apical dendrites, but not the basal (Fig. 8*E*). There were no significant differences in the total number of branch points between adult and old animals for any region of the dendritic tree (Fig. 8*G*). Finally, the density of dendritic spines was determined for a random 50-μm length of basal, apical tuft and primary (apical)

dendrites. In each of these regions, the number of dendrites per 50 μm length was significantly smaller for old animals than for adult ones (Fig. 9).

Discussion

In this paper, we compare basic synaptic, intrinsic, and morphological properties of thalamorecipient pyramidal neurons in S1 of adult and old rats. The major differences found in old rats were larger maximal EPSC amplitude; decreased suppression of IPSC amplitude during a train of stimuli, which partly resulted from decreased $GABA_B$ signaling; larger T-potentials; regional differences in dendritic complexity; and a decrease in dendritic spine density. For recent reviews on aging-related changes other species and cortical areas, see Peters and Kemper (2011) and Yeoman et al. (2012).

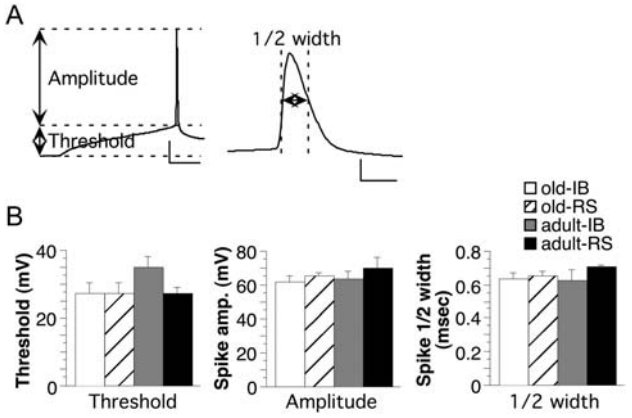

Figure 5. Characteristics of single action potentials. (*A*) Examples of single APs showing the measurement of threshold, amplitude (left) and half-width (right). Scale bars represent 20 mV and 20 ms (left) and 20 mV and 1 ms (right). (*B*) Quantification of AP threshold, amplitude and half-width for old versus adult and IB versus RS cells. $N = 21$ cells (11 IB and 10 RS) for old and 20 cells (6 IB and 14 RS) for adult.

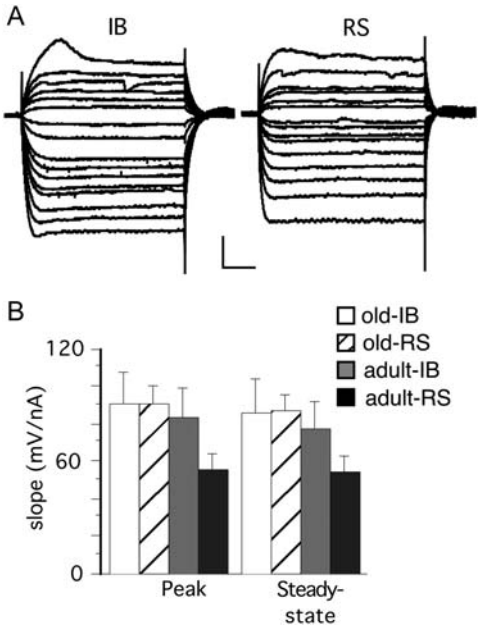

Figure 7. Properties of subthreshold responses. (*A*) Examples of subthreshold responses from an IB (left) and RS (right) cell to both hyperpolarizing and depolarizing current steps. Scale bars represent 10 mV and 100 ms. (*B*) Quantification of the mean slope of the I/O curve for the peak subthreshold response (left) and the steady-state measured at 400 ms after onset (right) for old versus adult and IB versus RS cells. $n = 21$ cells (11 IB and 10 RS) for old and 20 cells (6 IB and 14 RS) for adult.

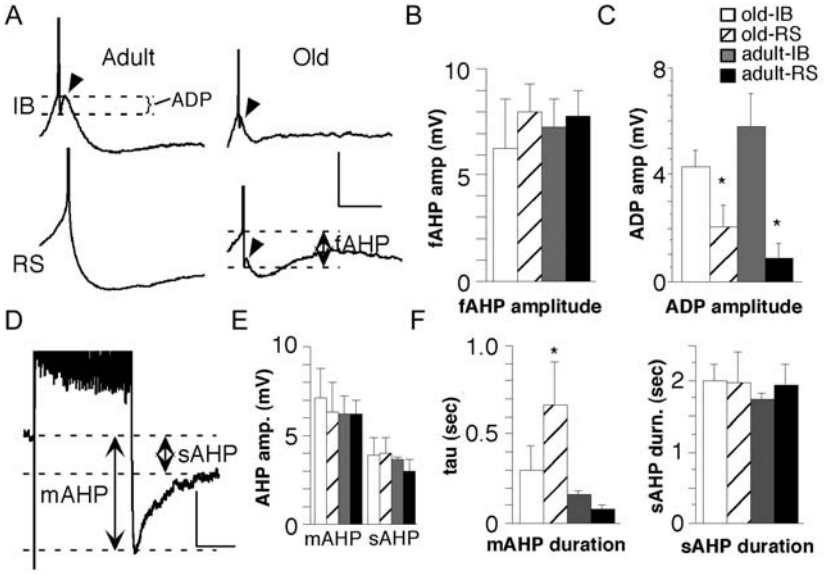

Figure 6. Characteristics of AHPs and ADPs. $N = 21$ cells (11 IB and 10 RS) for old and 20 cells (6 IB and 14 RS) for adult. (*A*) Examples of fAHPs and ADPs in adult (left traces) and old (right traces) animals for IB (top traces) and RS (bottom traces) cell types. The dotted lines show the measurement of ADPs (top left trace) and the fAHPs (bottom right trace). Arrowheads point to the ADP. Scale bars represent 10 mV and 50 ms. Note the APs are truncated. (*B*) Quantification of mean fAHP amplitude for old versus adult and IB versus RS cells. (*C*) Quantification of mean ADP amplitude for old versus adult and IB versus RS cells. Asterisks represent significant differences between the indicated mean and the other 3 means (1-way ANOVA, followed by Fisher's PLSD, $P > 0.05$). (*D*) Example of medium AHP (mAHP) and slow AHP (sAHP) after a train of APs and at −55 mV. The dotted lines show the measurement of the mAHP and sAHP. Scale bars represent 5 mV and 200 msec. Note APs are truncated. (*E*) Quantification of mean mAHP (left) and sAHP (right) amplitudes for old versus adult and IB versus RS cells. (*F*) Quantification of the mean durations of the mAHP (left) and sAHP (right). The asterisk represents significant difference between the indicated mean and the means of both categories of cells from adult rats (1-way ANOVA, followed by Fisher's PLSD, $P > 0.05$).

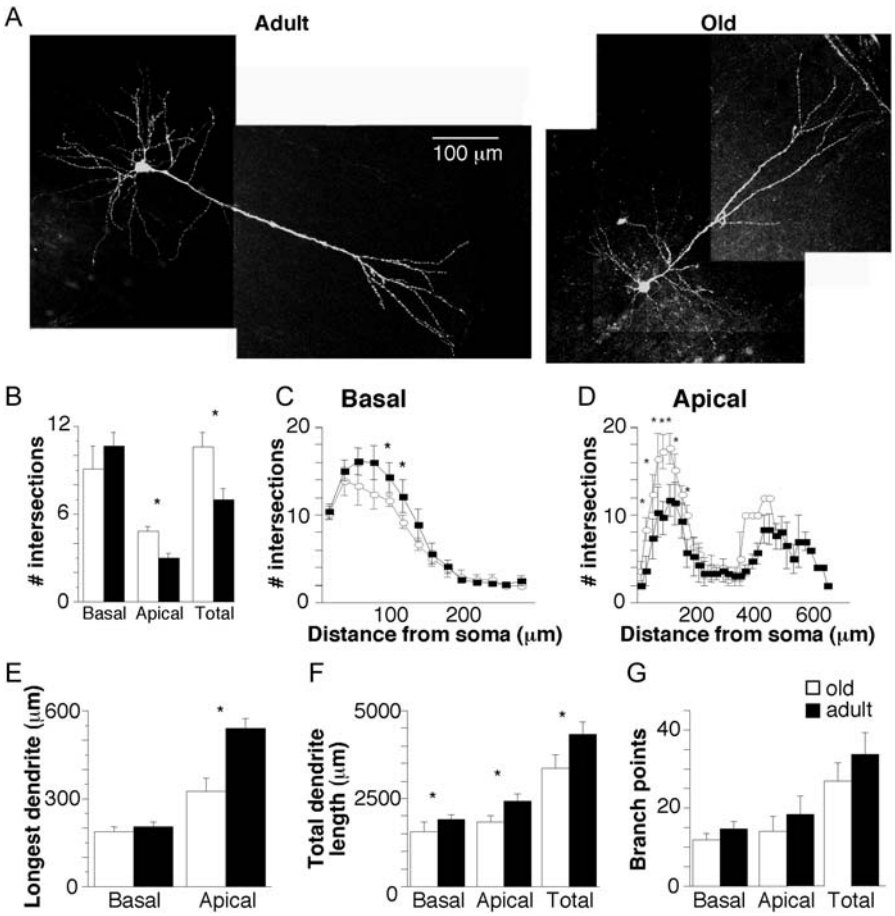

Figure 8. Characteristics of dendrites in old and adult animals. Note for each plot (B–G) the black bars represent data from adult animals and the white bars represent data from old animals; $n = 10$ cells for old and 11 cells for adult. Asterisks indicate significant differences ($P < 0.05$, unpaired *t*-test) between adult and old mean values. (*A*) Examples of deep layer 3 pyramidal neurons filled with biocytin during whole-cell recording in adult (left) and old (right) rat S1. (*B*) The mean total number of intersections with the concentric circles of the Scholl analysis (see Methods) is shown for basal (left), apical (middle), and total (right) dendrites. (*C*, *D*) The mean number of Scholl intersections is shown for each individual concentric circle (20 μm spacing) for basal dendrites (*C*) and apical dendrites (*D*) from adult (black squares) and old (white circles) rats. (*E*) The mean length of the longest dendrite is shown for basal (left) and apical (right) dendrites. (*F*) The total length of all dendrites is shown for basal (left), apical (middle), and total (right) dendrites. (*G*) The mean number of dendritic branch points is shown for basal (left), apical (middle), and total (right) dendrites.

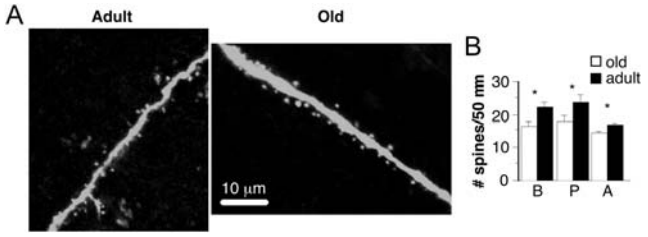

Figure 9. Dendritic spine densities in adult and old animals. (*A*) Examples of dendritic spines from the proximal apical dendrite from adult (left panel) and old (right panel) animals. (*B*) The mean density of dendritic spines (number of spines per 50 μm length of dendrite) is shown for basal ('B', left), proximal apical ('P', middle) and apical tuft ('A', right) dendrites from adult (black bars) and old (white bars) animals. $N = 10$ cells for old and 11 cells for adult. Asterisks indicate significant differences ($P < 0.05$, unpaired *t*-test) between adult and old mean values.

Hindpaw S1 was selected for analysis in this paper because this system has already provided a wealth of data on the changes in sensorimotor behavior and in S1 RF properties (Dinse 2006). Thus, the local-circuit analysis presented here is one of the few such analyses that can be directly related to higher levels of analysis in a well-defined system. One reason for focusing on the hindpaw system, rather than the forepaw, is that the effects of aging on the hindpaw behavior and responsiveness are large. Such changes during aging are much smaller for the forelimb and its representation in S1 (David-Jurgens et al. 2008).

Differences in Excitation and Inhibition

The resting potential and input resistance of cells in old and adult rats did not differ, as generally observed in other studies (Wong et al. 2000; Luebke et al. 2004); the values of these parameters were also similar to those previously observed (Hickmott and Merzenich 1998, 2002; Hickmott 2010). An interesting observation was that extracellular nifedipine was necessary to reliably voltage clamp cells at the EPSC reversal potential (~0 mV), particularly in old rats. In the absence of nifedipine, large persistent inward currents (L-channel) were observed that prevented accurate measurement of IPSCs (data not shown). This observation is consistent with other studies in the aged hippocampus, in which overall Ca^{2+} dysregulation is associated with an increase in L-channel density (Foster 2007). In other brain areas, notably cortex and basal ganglia, such an increase has not been documented (Kumar et al. 2009).

The individual EPSCs and IPSCs obtained here closely resemble those previously observed in slices from rodent S1 in terms of kinetics and amplitude (Fig. 1; Reyes et al. 1998; Finnerty et al. 1999; Fox 2008). Both EPSCs and IPSCs (Fig. 3) exhibited amplitude suppression during a train of stimuli. Similar EPSC suppression has been previously observed in juvenile S1 for thalamocortical responses and for cell pairs (Markram and Tsodyks 1996). The responses of juvenile S1 IPSPs to trains is variable, depending on the source and target of the inhibitory connection, but suppression was the most common outcome (Gupta et al. 2000; Markram et al. 2004). Horizontal connections (both excitatory and inhibitory) in adult S1 also exhibit mostly suppression, although to a lesser extent (Hickmott 2010). Such suppression for paired-pulse and steady-state conditions is typically attributed to presynaptic release properties (Markram and Tsodyks 1996; Dobrunz and Stevens 1997; Zucker and Regehr 2002). Thus, the observed decrease in suppression in old animals (Fig. 2) might suggest a decrease in GABA release probability with age. However, the observation that sPSCs did not differ in frequency between adult and old animals suggests that baseline release properties were not different. A major source of presynaptic suppression for cortical IPSCs is the activation of presynaptic $GABA_B$ receptors (Zucker and Regehr 2002). In our study, reduced suppression of IPSCs in old animals (Fig. 2) was correlated with a reduced effectiveness of a $GABA_B$ antagonist at short IPIs (Fig. 3). These data are consistent with the hypothesis that the amount of signaling through this receptor is less in old versus adult animals in S1. We further suggest that the most likely locus of the effect is presynaptic, particularly since postsynaptic $GABA_B$ currents were blocked by the Cs^+-based filling solution. This observation is consistent with previous data showing reductions in $GABA_B$ signaling in aged hippocampus (Billard et al. 1995) and inferior colliculus (Caspary et al. 2008).

Glutamate and GABA in Old Circuits

These data are consistent with measurements of glutamatergic and GABAergic transmission previously obtained by in vivo and in vitro methods. In general, levels of glutamate and the release of glutamate appear to be normal in aged cortex; for glutamate receptors, a general decrease in NMDA receptor density and a smaller and less consistent decrease in 2-amino-3-(5-methyl-3-oxo-1,2-oxazol-4-yl)propanoic acid (AMPA) receptor density have also been observed (Segovia et al. 2001). The density of dendritic spines and putative excitatory and inhibitory synapses also may decrease (Poe et al. 2001; Wong et al. 2006; Mora et al. 2007), although it has been suggested that inhibitory synapse density declines to a greater extent than excitatory (Poe et al. 2001). Electrophysiological studies in the cortex in vitro have demonstrated relative decreases in miniature EPSC frequency with aging (Wong et al. 2000; Luebke et al. 2004) and either increases (Luebke et al. 2004) or decreases (Wong et al. 2000) in miniature IPSC frequency. In the dentate gyrus of the hippocampus, the amplitude of EPSPs measured with field potentials and single-fiber EPSPs were larger in old rats, associated with an increase in quantal size (Barnes 1994; Rosenzwieg and Barnes 2003). These sorts of data are consistent with significant changes in presynaptic control of GABA release during aging and a postsynaptic increase in glutamatergic signaling. However, such results are region specific; for example, in the CA1 region of the hippocampus, there was a "reduction" in field EPSP amplitude with aging which was associated with a "decrease" in AMPA responsiveness (Barnes 1994; Rosenzweig and Barnes 2003).

Our data are consistent with the general idea of presynaptic changes in GABA transmission and postsynaptic changes in glutamate during aging. Physiological measures of presynaptic function (IPSC train suppression, CGP 55848 potency) differ for IPSCs, while markers of postsynaptic function (IPSC and sIPSC amplitude) do not differ. Measures of presynaptic EPSC function (sEPSC frequency, EPSC train suppression, CGP 55845 potency) do not differ, while markers of postysnaptic function (EPSC maximum amplitude, I/O slope) do differ. For IPSCs, it is interesting that sIPSC frequency was not increased with age, even though presynaptic release properties apparently changed. One explanation is that, in some systems, $GABA_B$ autoreceptor signaling is not manifest on single IPSCs, only on pairs and trains (Davies and Collingridge 1993), so that the change in $GABA_B$ signaling would not affect single spontaneous events or single IPSCs. Other studies have shown effects of $GABA_B$ blockers on sIPSCs that were attributed to activation of $GABA_B$ autoreceptors by ambient GABA (e.g. Kirmse and Kirischuk 2006). Thus, another possibility is that ambient GABA levels are low in the S1 slices from adult and old animals, and so the decrease in $GABA_B$ signaling with age does not affect sIPSCs or single IPSCs. In any case, the decrease in $GABA_B$ signaling observed could be due to changes in the autoreceptors themselves (e.g. density, sensitivity) or in the ability of those receptors to activate intracellular processes in GABA terminals.

Differences in Action Potential Properties

These pyramidal neurons could be categorized into 2 groups based on the presence (IB) or absence (RS) of a short burst of APs at the onset of the train. These categories of neurons have been observed previously in various cortical regions, where IB cells are most common in deeper cortical layers and mostly characteristic of pyramidal cells (Amitai and Connors 1995). The burst firing of some of these neurons has been attributed to the presence of the rapidly inactivating, low-threshold T-current (McCormick et al. 1985; Chen et al. 1996). We observed a similar T-potential that was larger in IB neurons (Fig. 4*B*, *C*); when it was blocked cells were converted from IB to RS firing (Fig. 4E), as has been observed previously (McCormick et al. 1985; Chen et al. 1996). Neurons from old S1 were more likely to exhibit IB firing and showed a larger T-potential (Fig. 4). When the cells were separated into IB and RS types, the T-potential proved larger in IB than RS cells for both old and adult animals, but was only larger for old animals in RS cells (Fig. 4*C*). Thus, the data suggest that the transition from RS to IB firing depends on a certain threshold level of T-current being reached, and once that threshold is reached the neuron changes from RS to IB. As RS neurons in old S1 have larger T-potentials (Fig. 4*C*), we hypothesize that more RS cells reach this "threshold" during aging and are converted into IB cells. Interestingly, the amplitude of the ADP, which is thought to reflect activation of a persistent Na^+ current (Nishimura et al. 2001), showed a similar pattern to the T-potential (Fig. 6*C*). Thus, either the ADP is regulated in a similar manner as the T-potential during aging, or the ADP is dependent on the T-potential for

activation. The fact that the ADP was not significantly reduced by depolarization (data not shown) and the T-potential was (Fig. 4*E*) supports the first possibility. Note that similar increases in T-current have been documented in aged basal forebrain (Murchison and Griffith 1995) but not in hippocampus or cortex (Kumar et al. 2009).

On the basis of the maximum firing rate (Fig. 4*F*) and slope of the I/O curve for APs (Fig. 4*G*), there was little overall change in excitability in old animals. Previous data from frontal cortex have indicated that there can be changes in overall excitability, but they are restricted to layer 2/3 cells, not layer 5 cells (Chang et al. 2005; Luebke and Chang 2007). In hippocampus, a general decrease in AP excitability has been observed (Foster et al. 2007). In primary visual cortex, extracellular recordings have documented increases in AP rate (Schmolesky et al. 2000; Leventhal et al. 2003). Thus, overall, it is clear that changes in excitability with aging are cell and region specific and may reflect either functional or homeostatic changes in neurons. One posited role for bursting neurons is to amplify highly synchronous inputs (e.g. Chagnac-Amitai and Connors 1989). As one consequence of aging is demyelination of peripheral sensory afferents (Dinse 2006), which would most likely decrease input synchrony to S1, this increase in numbers of IB cells may be an example of homeostatic plasticity, with the cortical circuit trying to enhance the remaining synchronous inputs by using IB cells.

Some of the differences in AP excitability previously described have been attributed to differences in AHP properties, particularly sAHPs. As the sAHP is mediated by a Ca^{2+}-activated K^+ current, this is thought to reflect the increase in Ca^{2+} flux through L-type channels (Foster 2007). Even though such an increase in L-channel function was observed in this study (see above), no corresponding increase in mAHP or sAHP amplitude was observed (Fig. 6*E*, right). However, the duration of the mAHP was increased (Fig. 6*F*). Furthermore, no differences were observed in single AP properties, threshold, amplitude, and duration (Fig. 5). Again, as for overall excitability, it is clear that the regulation of these properties is cell-type specific, as they do vary with age in other cells (Foster 2007).

Changes in Dendrites and Spines

Changes in dendritic architecture, including dendritic spines have been consistently observed during aging. Initially, it was thought that the general decrease in gray matter extent during aging reflected general dendritic hypotrophy. However, observations of single neurons indicate that neurons often show reductions or stability of their dendrites during aging; however, they may show increases in dendritic length in specific regions (Coleman and Flood 1987; Burke and Barnes 2006). Dendrites and dendritic spines have been recently assessed in old rat sensorimotor cortex (Wang et al. 2009) with similar overall results to those shown here. However, when the Scholl data were assessed separately in basal and apical dendrites, as shown in Figure 8*C* and *D*, more intersections were observed in adult animals only for basal dendrites close to the soma; apical dendrites showed more intersections close to the soma for old animals. Thus, our more detailed analysis revealed additional complexity in the regulation of dendritic complexity in old S1. The bulk of the thalamocortical synapses onto layer 2/3 pyramidal cells are thought to be made with basal dendrites, as are the intracortical synapses from adjacent layer 2/3 pyramids (Feldmeyer et al. 2006). Thus, the target area for such synapses was decreased in the old animals (Fig. 8*C*). The population of dendrites that are enhanced in complexity in old animals was also relatively close to the soma (Fig. 8*D*), and also receive primarily intracortical connections. How these 2 sets of connections might differ and why such a difference would be differentially modulated by aging remain to be determined. One interesting possibility is that the total dendritic extent may be negatively coregulated, with apical and basal dendrites competing for some factor or factors that enhance growth; thus, retractions of dendrites in one region of a neuron would lead to compensatory increases in other regions (Samsonovich and Ascoli 2006), as was observed here.

Previous studies have demonstrated a reduction in spine density in old rat sensorimotor cortex (Wang et al. 2009), as well as human (de Brabander et al. 1998; Duan et al. 2003) and non-human primate cortex (Page et al. 2002). The extent of spine loss in aged hindpaw S1 shown in Figure 9 is comparable to those observed previously (Wang et al. 2009). The loss of spines, as the targets for excitatory terminals, will decrease the overall excitation of the neuron; such a decrease could invoke compensatory homeostatic plasticity of excitatory synapses, leading to an increase overall excitability, as was observed (Fig. 1). As both spines and dendrites can be affected by changes in activity in adult cortex (Trachtenberg et al. 2002; Hickmott and Steen 2005; Tailby et al. 2005), the changes in activity patterns themselves may also contribute to the structural changes observed.

Relationship to Responses to Tactile Stimulation of the Hindpaw

Previous data from rat hindpaw S1 have shown that the disruption in hindpaw gait observed in aged rats is correlated with significant expansion of the RFs recorded in S1 (Spengler et al. 1995; Godde et al. 2002; David-Jurgens et al. 2008). More recently, temporal aspects of these S1 responses have been examined with paired (David-Jurgens and Dinse 2010) and train stimuli (David-Jurgens and Dinse 2008) in old animals. Paired tactile stimulation of the hindpaw leads to a depression of the second response with respect to the first (paired-pulse depression) in both adult and old S1. The PPRs were found to be larger in old rats; however, the underlying cause of the increase appeared to be a decrease in responsiveness to the first pulse (David-Jurgens and Dinse 2010). At first glance, it appears that observation is not consistent with the data presented here showing an increase in the amplitude of thalamocortical EPSCs (Fig. 1) and an increase in early burst firing (Fig. 4), which would be expected to increase the overall spike response. However, Jürgen-David and Dinse hypothesized that the decrease in the first response was due to changes in subcortical processes, possibly the pronounced decreased in conduction velocity of sensory afferents, which would lead to a decrease in the synchrony of incoming sensory inputs and a decrease in the response (Bruno and Sakmann 2006). Such a decrease in synchrony would result in reduced excitatory drive to the thalamocortical afferents and a reduction in responsiveness. Such a reduction in thalamocortical drive might then lead to a compensatory increase

in excitability of EPSCs and APs by a homeostatic process (Turrigiano 1999).

Trains of tactile stimuli lead to response suppression across the train as measured by spiking responses in S1. The effect of aging on this suppression was complex: in two-thirds of the animals, the amount of suppression observed for short ISIs was approximately the same as in adult animals ("unimpaired"); in the other third, the amount of suppression was increased with a large increase in variance ("impaired"; David-Jurgens and Dinse 2008). One possibility for this increase in suppression would be an increase in inhibition (decrease in inhibitory suppression) across the train, as was observed in this study (Fig. 2). It is unlikely to explain the separation of old animals into 2 categories, however, because enhanced suppression was observed for all IPSCs (data not shown). Overall, then, the effects of aging on the synaptic and intrinsic properties examined in this paper explain some but not all of the changes in responses observed in intact hindpaw S1.

Receptive Fields, Excitation and Inhibition

Many sensorimotor and cognitive abilities decline with age. The neural circuit changes underlying these deficits are largely unknown, but disruption of the normal balance of excitation and inhibition has been hypothesized to play an important role. In the somatosensory system, degradation of spatial RFs is correlated with reduced function in rodents (Godde et al. 2002) and humans (Kalisch et al. 2009). The temporal response properties of S1 neurons can also be impaired (David-Jurgens and Dinse 2008). Recent studies in humans (Lenz et al. 2012) have documented a decrease in paired-pulse suppression of somatosensory-evoked potentials that is correlated with degradation of tactile acuity. In monkey primary visual cortex (V1) the decline in visual function during aging is correlated with degradation of RF properties (e.g. orientation and direction selectivity; Schmolesky et al. 2000). Also, the ability of cells in V1 to follow trains of flashing light was impaired in old animals (Mendelson and Wells 2002). Similarly, in adult auditory cortex (A1) cells respond well to rapid tone repetition rates, while cells in old A1 respond best to slow rates (Mendelson and Ricketts 2001). The spatial and temporal properties of RFs are shaped by the balance of excitation and inhibition, with inhibition particularly important in constraining the size of RFs (Hicks et al. 1986; Chowdhury and Rasmusson 2002). Direct evidence for a reduction in GABAergic inhibition has been obtained in V1 by Leventhal et al. (2003). They demonstrated that GABA antagonists have reduced effects on V1 RFs in aged monkeys and that infusion of GABA into the cortex could "rescue" properties of old RFs, making them more closely resemble adult RFs. Our data are consistent with a specific reduction in $GABA_B$-mediated inhibition, which is likely most closely related to deficits in temporal rather than spatial inhibition.

Temporal properties of cortical circuits are also greatly affected by the balance of excitation and inhibition. In particular, both excitatory and inhibitory synaptic events can either depress or facilitate during a high-frequency train. Thus, the overall response during a train will depend on the relative changes in excitation and inhibition. The observation that thalamocortical IPSCs in old S1 show reduced suppression across a train (Fig. 2) indicates that the normal balance of excitation and inhibition, particularly for steady-state stimuli, can be disrupted during aging and tend toward too much inhibition. Similar decreases have been observed and in the auditory systems are thought to play a role in disruption of normal temporal processing and response reliability (Caspary et al. 2008).

Funding

Supported by a grant to H.D. from the Deutsche Forschungsgemeinschaft—DFG (Di 334/19-1).

References

Amitai Y, Connors BW. 1995. Intrinsic physiology and morphology of single neurons in neocortex. In: Jones EG, Diamond IT, editors. Cerebral cortex. New York: Plenum Press.

Barnes CA. 1994. Normal aging: regionally specific changes in hippocampal synaptic transmission. Trends Neurosci. 17:13–18.

Billard JM, Lamour Y, Dutar P. 1995. Decreased monosynaptic $GABA_B$-mediated inhibitory postsynaptic potentials in hippocampal CA1 pyramidal cells in the aged rat: pharmacological characterization and possible mechanisms. J Neurophysiol. 74:539–546.

Blanton MG, LoTurco JJ, Kriegstein AR. 1989. Whole cell recordings from neurons in slices of reptilian and mammalian cortex. J Neurosci Meth. 30:203–210.

Bruno RM, Sakmann B. 2006. Cortex is driven by weak but synchronously active thalamocortical synapses. Science. 312:1622–1627.

Burke SN, Barnes CA. 2006. Neural plasticity in the ageing brain. Nat Rev Neurosci. 7:30–40.

Caspary DM, Ling L, Turner JG, Hughes LF. 2008. Inhibitory neurotransmission, plasticity and aging in the mammalian central auditory system. J Exp Biol. 211:1781–1791.

Chagnac-Amitai Y, Connors BW. 1989. Synchronized excitation and inhibition driven by intrinsically bursting neurons in neocortex. J Neurophshiol. 62:1149–62.

Chang YM, Rosene DL, Killiany RJ, Mangiamele LA, Luebke JI. 2005. Increased action potential firing rates of layer 2/3 pyramidal cells in the prefrontal cortex are significantly related to cognitive performance in aged monkeys. Cereb Cortex. 15:409–418.

Chen W, Zhang J-J, Hu G-Y, Wu C-P. 1996. Electrophysiological and morphological properties of pyramidal and nonpyramidal neurons in the cat motor cortex in vitro. Neuroscience. 73:39–55.

Chowdhury SA, Rasmusson DD. 2002. Comparison of receptive field expansion produced by GABA(B) and GABA(A) receptor antagonists in raccoon primary somatosensory cortex. Exp Brain Res. 144:114–121.

Coleman PD, Flood DG. 1987. Neuron numbers and dendritic extent in normal aging and Alzheimer's disease. Neurobiol Aging. 8:521–545.

David-Jurgens M, Churs L, Berkefeld T, Zepka RF, Dinse HR. 2008. Differential effects of aging on fore- and hindpaw maps of rat somatosensory cortex. PLoS ONE. 3:e3399.

David-Jurgens M, Dinse HR. 2008. Age related alterations of response properties of cortical somatosensory neurons after presentation of train stimuli - influence of age on temporal processing. 2008 Abstract viewer/itinerary planner. Washington, DC: Society for Neuroscience.

David-Jurgens M, Dinse HR. 2010. Effects of aging on paired-pulse behavior of rat somatosensory cortical neurons. Cereb Cortex. 20:1208–1216.

Davies CH, Collingridge GL. 1993. The physiological regulation of synaptic inhibition by GABAB autoreceptors in rat hippocampus. J Physiol. 472:245–265.

de Brabander JM, Kramers RJ, Uylings HB. 1998. Layer-specific dendritic regression of pyramidal cells with ageing in the human prefrontal cortex. Eur J Neurosci. 10:1261–1269.

DiCarlo JJ, Lane JW, Hsiao SS, Johnson KO. 1996. Marking microelectrode penetrations with fluorescent dyes. J Neurosci Methods. 64:75–81.
Dinse HR. 2006. Cortical reorganization in the aging brain. Prog Brain Res. 157:57–80.
Dobrunz LE, Stevens CF. 1997. Heterogeneity of release probability, facilitation, and depletion at central synapses. Neuron. 18:995–1008.
Duan H, Wearne SL, Rocher AB, Macedo A, Morrison JH, Hof PR. 2003. Age-related dendritic and spine changes in corticocortically projecting neurons in macaque monkeys. Cereb Cortex. 13:950–961.
Dustman RE, Emmerson RY, Shearer DE. 1996. Life span changes in electrophysiological measures of inhibition. Brain Cogn. 30:109–126.
Feldmeyer D, Lubke J, Sakmann B. 2006. Efficacy and connectivity of intracolumnar pairs of layer 2/3 pyramidal cells in the barrel cortex of juvenile rats. J Physiol. 575:583–602.
Finnerty GT, Roberts LS, Connors BW. 1999. Sensory experience modifies the short-term dynamics of neocortical synapses. Nature. 400:367–371.
Foster TC. 2007. Calcium homeostasis and modulation of synaptic plasticity in the aged brain. Aging Cell. 6:319–325.
Fox K. 2008. Barrel cortex. Oxford: Oxford University Press.
Galarreta M, Hestrin S. 1998. Frequency-dependent synaptic depression and the balance of excitation and inhibition in the neocortex. Nat Neurosci. 1:587–594.
Godde B, Berkefeld T, David-Jurgens M, Dinse HR. 2002. Age-related changes in primary somatosensory cortex of rats: evidence for parallel degenerative and plastic-adaptive processes. Neurosci Biobehav Rev. 26:743–752.
Gupta A, Wang Y, Markram H. 2000. Organizing principles for a diversity of GABAergic interneurons and synapses in the neocortex. Science. 287:273–278.
Hickmott PW. 2010. Synapses of horizontal connections in adult rat somatosensory cortex have different properties depending on the source of their axons. Cereb Cortex. 20:591–601.
Hickmott PW, Merzenich MM. 1998. Single-cell correlates of a representational boundary in rat somatosensory cortex. J Neurosci. 18:4403–4416.
Hickmott PW, Merzenich MM. 1999. Dendritic bias of neurons in rat somatosensory cortex associated with a functional boundary. J Comp Neurol. 409:385–399.
Hickmott PW, Merzenich MM. 2002. Local circuit properties underlying cortical reorganization. J Neurophysiol. 88:1288–1301.
Hickmott PW, Steen PA. 2005. Large-scale changes in dendritic structure during reorganization of adult somatosensory cortex. Nat Neurosci. 8:140–142.
Hicks TP, Metherate R, Landry P, Dykes RW. 1986. Bicuculline-induced alterations of response properties in functionally identified ventroposterior thalamic neurones. Exp Brain Res. 63:248–264.
Jürgens M, Dinse HR. 1998. Distribution of the calcium-binding protein parvalbumin in the fore- and hindpaw ,representation of somatosensory cortex of adult and aged rats. Soc Neurosci Abstr. 24:633.
Kalisch T, Ragert P, Schwenkreis P, Dinse HR, Tegenthoff M. 2009. Impaired tactile acuity in old age is accompanied by enlarged hand representations in somatosensory cortex. Cereb Cortex. 19:1530–1538.
Kirmse K, Kirischuk S. 2006. Ambient GABA constrains the strength of GABAergic synapses at Cajal-Retzius cells in the developing visual cortex. J Neurosci. 26:4216–4227.
Kumar A, Bodhinathan K, Foster TC. 2009. Susceptibility to calcium dysregulation during brain aging. Front Aging Neurosci. 1:1–13.
Lenz M, Tegenthoff M, Kohlhaas K, Stude P, Höffken O, Gatica Tossi MA, Kalisch T, Dinse HR. 2012. Increased excitability of somatosensory cortex in aged humans is associated with impaired tactile acuity. J Neurosci. 32:1811–1816.
Leventhal AG, Wang Y, Pu M, Zhou Y, Ma Y. 2003. GABA and its agonists improved visual cortical function in senescent monkeys. Science. 300:812–815.
Luebke JI, Chang YM. 2007. Effects of aging on the electrophysiological properties of layer 5 pyramidal cells in the monkey prefrontal cortex. Neuroscience. 150:556–562.
Luebke JI, Chang YM, Moore TL, Rosene DL. 2004. Normal aging results in decreased synaptic excitation and increased synaptic inhibition of layer 2/3 pyramidal cells in the monkey prefrontal cortex. Neuroscience. 125:277–288.
Markram H, Toledo-Rodriguez M, Wang Y, Gupta A, Silberberg G, Wu C. 2004. Interneurons of the neocortical inhibitory system. Nat Rev Neurosci. 5:793–807.
Markram H, Tsodyks M. 1996. Redistribution of synaptic efficacy between neocortical pyramidal neurons. Nature. 382:807–810.
McCormick DA, Connors BW, Lighthall JW, Prince DA. 1985. Comparative electrophysiology of pyramidal and sparsely spiny stellate neurons of the neocortex. J Neurophysiol. 54:782–806.
Mendelson JR, Ricketts C. 2001. Age-related temporal processing speed deterioration in auditory cortex. Hear Res. 158:84–94.
Mendelson JR, Wells EF. 2002. Age-related changes in the visual cortex. Vision Res. 42:695–703.
Mora F, Segovia G, del Arco A. 2007. Aging, plasticity and environmental enrichment: structural changes and neurotransmitter dynamics in several areas of the brain. Brain Res Rev. 55:78–88.
Murchison D, Griffith WH. 1995. Low-voltage activated calcium currents increase in basal forebrain neurons from aged rats. J Neurophysiol. 74:876–887.
Nishimura Y, Asahi M, Saitoh K, Kitagawa H, Kumazawa Y, Itoh K, Lin M, Akamine T, Shibuya H, Asahara T *et al.* 2001. Ionic mechanisms underlying burst firing of layer III sensorimotor cortical neurons of the cat: an in vitro slice study. J Neurophysiol. 86:771–781.
Page TL, Einstein M, Duan H, He Y, Flores T, Rolshud D, Erwin JM, Wearne SL, Morrison JH, Hof PR. 2002. Morphological alterations in neurons forming corticocortical projections in the neocortex of aged Patas monkeys. Neurosci Lett. 317:37–41.
Peters A, Kemper T. 2011. A review of the structural alterations in the cerebral hemispheres of the aging rhesus monkey. Neurobiol Aging. Epub ahead of print.
Poe BH, Linville C, Brunso-Bechtold J. 2001. Age-related decline of presumptive inhibitory synapses in the sensorimotor cortex as revealed by the physical disector. J Comp Neurol. 439:65–72.
Reyes A, Lujan R, Rozov A, Burnashev N, Somogyi P, Sakmann B. 1998. Target-cell-specific facilitation and depression in neocortical circuits. Nat Neurosci. 1:279–285.
Rosenzweig ES, Barnes CA. 2003. Impact of aging on hippocampal function: plasticity, network dynamics, and cognition. Prog Neurobiol. 69:143–179.
Sah P. 1996. Ca2+-activated K+ currents in neurones: types, physiological roles and modulation. Trends Neurosci. 19:150–154.
Samsonovich AV, Ascoli GA. 2006. Morphological homeostasis in cortical dendrites. Proc Natl Acad Sci USA. 103:1569–1574.
Schmolesky MT, Wang Y, Pu M, Leventhal AG. 2000. Degradation of stimulus selectivity of visual cortical cells in senescent rhesus monkeys. Nat Neurosci. 3:384–390.
Segovia G, Porras A, Del Arco A, Mora F. 2001. Glutamatergic neurotransmission in aging: a critical perspective. Mech Ageing Dev. 122:1–29.
Shepherd GM. 2004. The synaptic organization of the brain, 5th ed. Oxford: Oxford University Press.
Spengler F, Godde B, Dinse HR. 1995. Effects of ageing on topographic organization of somatosensory cortex. Neuroreport. 6:469–473.
Tailby C, Wright LL, Metha AB, Calford MB. 2005. Activity-dependent maintenance and growth of dendrites in adult cortex. Proc Natl Acad Sci USA. 102:4631–4636.
Trachtenberg JT, Chen BE, Knott GW, Feng G, Sanes JR, Welker E, Svoboda K. 2002. Long-term in vivo imaging of experience-dependent synaptic plasticity in adult cortex. Nature. 420:788–794.
Turrigiano GG. 1999. Homeostatic plasticity in neuronal networks: the more things change, the more they stay the same. Trends Neurosci. 22:221–227.

Wang TJ, Chen JR, Wang YJ, Tseng GF. 2009. The cytoarchitecture and soma-dendritic arbors of the pyramidal neurons of aged rat sensorimotor cortex: an intracellular dye injection study. Neuroscience. 158:776–785.

Weiss T, Miltner WH, Liepert J, Meissner W, Taub E. 2004. Rapid functional plasticity in the primary somatomotor cortex and perceptual changes after nerve block. Eur J Neurosci. 20:3413–3423.

Wong TP, Marchese G, Casu MA, Ribeiro-da-Silva A, Cuello AC, De Koninck Y. 2006. Imbalance towards inhibition as a substrate of aging-associated cognitive impairment. Neurosci Lett. 397:64–68.

Wong TP, Marchese G, Casu MA, Ribeiro-da-Silva A, Cuello AC, De Koninck Y. 2000. Loss of presynaptic and postsynaptic structures is accompanied by compensatory increase in action potential-dependent synaptic input to layer V neocortical pyramidal neurons in aged rats. J Neurosci. 20:8596–8606.

Yeoman M, Scutt G, Faragher R. 2012. Insights into CNS ageing from animal models of senescence. Nat Rev Neurosci. 13:435–445.

Zucker RS, Regehr WG. 2002. Short-term synaptic plasticity. Annu Rev Physiol. 64:355–405.